NREL
NATIONAL RENEWABLE ENERGY LABORATORY

Absorber Alignment Measurement Tool for Solar Parabolic Trough Collectors

Preprint

J. Kathleen Stynes
University of Colorado at Boulder

Benjamin Ihas
National Renewable Energy Laboratory

To be presented at the ASME 2012 6th International Conference on Energy Sustainability & 10th Fuel Cell Science, Engineering and Technology Conference
San Diego, California
July 23–26, 2012

Conference Paper
NREL/CP-5500-54214
April 2012

Contract No. DE-AC36-08GO28308

Available electronically at http://www.osti.gov/bridge

Available for a processing fee to U.S. Department of Energy
and its contractors, in paper, from:

U.S. Department of Energy
Office of Scientific and Technical Information
P.O. Box 62
Oak Ridge, TN 37831-0062
phone: 865.576.8401
fax: 865.576.5728
email: mailto:reports@adonis.osti.gov

Available for sale to the public, in paper, from:

U.S. Department of Commerce
National Technical Information Service
5285 Port Royal Road
Springfield, VA 22161
phone: 800.553.6847
fax: 703.605.6900
email: orders@ntis.fedworld.gov
online ordering: http://www.ntis.gov/help/ordermethods.aspx

Cover Photos: (left to right) PIX 16416, PIX 17423, PIX 16560, PIX 17613, PIX 17436, PIX 17721

Printed on paper containing at least 50% wastepaper, including 10% post consumer waste.

ABSORBER ALIGNMENT MEASUREMENT TOOL FOR SOLAR PARABOLIC TROUGH COLLECTORS

J. Kathleen Stynes
Department of Mechanical Engineering
University of Colorado at Boulder
Boulder, Colorado 80301
Email: stynesj@colorado.edu

Benjamin Ihas
Thermal Systems Group
National Renewable Energy Laboratory
Golden, Colorado, 80401
Benjamin.Ihas@nrel.gov

ABSTRACT

As we pursue efforts to lower the capital and installation costs of parabolic trough solar collectors, it is essential to maintain high optical performance. While there are many optical tools available to measure the reflector slope errors of parabolic trough solar collectors, there are few tools to measure the absorber alignment. A new method is presented here to measure the absorber alignment in two dimensions to within 0.5 cm. The absorber alignment is measured using a digital camera and four photogrammetric targets. Physical contact with the receiver absorber or glass is not necessary. The alignment of the absorber is measured along its full length so that sagging of the absorber can be quantified with this technique. The resulting absorber alignment measurement provides critical information required to accurately determine the intercept factor of a collector.

NOMENCLATURE

η_o Optical efficiency
γ Intercept factor
ρ Reflectance
τ Transmittance
α Absorptance
θ_{a} Effective slope error
$X_{\mathrm{t}}, Y_{\mathrm{t}}, Z_{\mathrm{t}}$ A point on the parabolic trough reflector
$X_{\mathrm{a}}, Z_{\mathrm{a}}$ Location of the absorber
f Focal length of the parabolic trough collector
w_{ap} Aperture width of the parabolic trough collector
l_{c} Length of the parabolic trough collector
$X_{\mathrm{c}}, Y_{\mathrm{c}}, Z_{\mathrm{c}}$ Location of the camera
$\theta_\alpha, \theta_\beta, \theta_\gamma$ Euler rotation angle of camera
$X_{\mathrm{f}}, Z_{\mathrm{f}}$ Projection of the absorber onto the focal-line plane
$X_{\mathrm{p}}, Y_{\mathrm{p}}, Z_{\mathrm{p}}$ A point in object space
$x'_{\mathrm{p}}, y'_{\mathrm{p}}$ Image point on real camera sensor
$x_{\mathrm{p}}, y_{\mathrm{p}}$ Image point on ideal camera sensor
$\delta_{\mathrm{x}}, \delta_{\mathrm{y}}$ Total lens distortion components
x_0, y_0 Principal point on the image sensor
f_{c} Focal length of the camera
$s_{\mathrm{x}}, s_{\mathrm{y}}$ Height and length of the image sensor
$N_{\mathrm{p_x}}, N_{\mathrm{p_y}}$ Number of pixels along each side of image sensor
$x_{\mathrm{I}}, y_{\mathrm{I}}$ Index location of a pixel in a photograph
$(X_{\mathrm{p}i}, Y_{\mathrm{p}i}, Z_{\mathrm{p}i})$ Photogrammetry target locations
$d_{i,j}$ Distance measurements between photogrammetry targets

INTRODUCTION

Parabolic solar collectors are designed for a receiver absorber aligned with the focal line of the parabola. An absorber is considered misaligned if, at any point along its length, the center of the absorber deviates from the focal line of the parabolic trough. Absorbers may be misaligned due to poor structural design, poor installation, sag from the weight of the heat transfer fluid and the tube itself, or change in the structure over time due to wind loading or other effects. Absorber misalignments contribute significantly to reductions in optical performance, but are often underestimated or ignored in modeling. To measure

the absorber alignment of parabolic solar collectors, we have developed a simple measurement technique that can be employed without any special equipment beyond a digital camera. This technique requires two digital photographs of the collector and absorber taken from opposite sides of the aperture.

Previous Work

The importance of accurate absorber alignment was recognized with the development of the first parabolic trough collectors. The dependence of overall collector efficiency on absorber alignment was modeled at Sandia National Laboratories by [1] during the development and installation of parabolic trough collectors in Albuquerque, NM. This work was later expanded upon at Sandia with a report detailing the effects of absorber location on parabolic trough annual performance [2]. Despite the recognition of the importance of the absorber alignment in optical modeling, there has been little effort to measure the absorber location of parabolic trough collectors in the field or laboratory. Reports exist describing the use of a laser distance meter to determine this location [3]; however, descriptions regarding the process, difficulty, and accuracy are incomplete and ignore the complications of laser-probing a highly absorptive surface through glass. Additionally, the receiver glass envelope location has been measured relative to the reflector surface using photogrammetry [4]. For this technique, eight photogrammetry targets are placed on the receiver glass; the target locations are measured using 75 photographs and an additional 14,000 targets placed on the reflector surface. The target positional precision is reported as $\sigma = 0.14$ mm for the targets on the glass. While it is very precise, this method is also fairly tedious, requiring a large number of photographs and the placement of targets on the receiver glass, and it has the disadvantage of not explicitly determining the absorber location. Neither of these methods are the focus of the work in which they are presented but rather a supplement to the measurement of reflector slope errors.

1 Theory

1.1 Intercept Factor

To gain appreciation for the importance of absorber alignment, it is helpful to understand how it affects the overall collector efficiency. The efficiency of a concentrating solar collector varies with the level of direct-normal solar radiation and the absorber temperature. However, due to the difficulty of measuring the absorber temperature directly, the efficiency is usually expressed as a function of the heat transfer fluid temperature with a single curve for each level of direct-normal solar radiation. As shown in Fig. 1, the optical losses far outweigh the thermal losses in the typical operating temperature range. Absorber misalignment contributes directly to the optical losses.

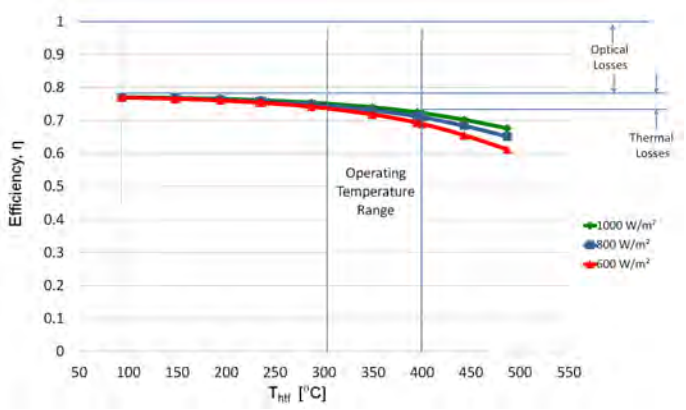

FIGURE 1. EFFICIENCY CURVE FOR PARABOLIC SOLAR COLLECTOR COMPARING OPTICAL LOSSES TO THERMAL LOSSES

Because the thermal and optical efficiencies behave nearly independently, the optical performance of a solar concentrator can be treated separately from the thermal performance. The optical efficiency at normal incidence is the product of the intercept factor γ, the mirror reflectance ρ, the glass transmittance τ, and the absorber absorptance α.

$$\eta_o = \gamma \rho \tau \alpha \tag{1}$$

While the reflectance, transmittance, and absorptance are material properties that can be measured in a laboratory, the intercept factor is a purely geometric quantity that characterizes the total geometric accuracy of the system and is defined as the fraction of solar energy reflected from the concentrator that is intercepted by the absorber tube.

The intercept factor depends on several components including the reflector's surface profile or slope, reflector's specularity, reflector's alignment, absorber's alignment, and the system's solar tracking error. Additionally, factors that influence the intercept factor that are difficult to measure or dynamic in time include wind loading, gravitational loading, and sun shape. While the intercept factor is of utmost significance when evaluating the performance of a parabolic solar collector, it is extremely difficult to measure due to its many contributing factors. Of all these factors, the greatest emphasis is usually placed on the reflector's profile, characterized by surface slope. Several optical tools exist to measure the slope errors of the reflecting surface including VSHOT [5], SOFAST [6], photogrammetry [7], and TARMES [3]. Table 1 summarizes the main techniques for measuring the reflector's slope error and how each treats the absorber. Upon measuring the reflector's slope, an estimate of the collector's intercept factor is often presented with the results. The other

TABLE 1. REFLECTOR SLOPE ERROR MEASUREMENT TOOLS AND CORRESPONDING TREATMENT OF THE ABSORBER

Tool or Technique	Method to Locate Absorber
TARMES (reflected image analysis) [3]	Laser distance meter
Photogrammetry [4]	Targets affixed to glass envelope
VSHOT (point reflection) [5]	Assumed ideal position
SOFAST (fringe deflectometry) [6]	Assumed ideal position
TOPCAT (reflected image analysis) [12]	Camera and boresight gauge

parameters included in the intercept factor are typically estimated at the researcher's discretion. There is no standard regarding the inclusion of specific parameters, let alone their default values. While it may not be realistic to measure each of these parameters for each different collector due to the experimental difficulty in evaluating them, the absorber misalignment can now be measured quite simply and accurately. Absorber misalignments as small as 1.0 cm have the equivalent effect of slope errors as significant as 3 mrad for an LS-2 geometry. It is thus prudent to include absorber misalignment in any intercept factor calculation, and, when possible, measure the actual absorber misalignment in addition to the reflector's slope errors to provide an accurate intercept factor.

1.2 Effects of Absorber Misalignment

To provide an understanding of the significance of absorber misalignments relative to slope errors in the reflector surface, it is convenient to model absorber misalignment as a distribution of effective slope errors. For a perfect reflector with no surface slope errors, an incoming ray, assumed to be parallel to the optical axis, will be reflected and pass through the focal point of the parabola as shown in Fig. 2 (labeled as "ideal reflection"). For an incoming ray to pass through the center of an absorber tube that is not aligned with the focal point, the reflector surface must have nonzero slope error. An absorber misalignment can thus be modeled as a perfectly aligned absorber and a set of effective slope errors in the reflector surface. The effective slope error, θ_a, at each point across the aperture is determined by finding the surface slope error required for an incoming solar ray to intersect the center of the absorber instead of the focal point. The effective slope error is equal to half of the angle between the absorber tube, the point on the aperture, and the focal point as shown in Fig. 2. For a known absorber location, (X_a, Z_a), the effective slope error at a point on the parabolic trough reflector, (X_t, Z_t), of a parabolic collector with focal point $(0, f)$ is calculated using Eqn. 2.

$$\theta_a = \frac{1}{2}\left[\tan^{-1}\left(\frac{X_t - 0}{Z_t - f}\right) - \tan^{-1}\left(\frac{X_t - X_a}{Z_t - Z_a}\right)\right] \qquad (2)$$

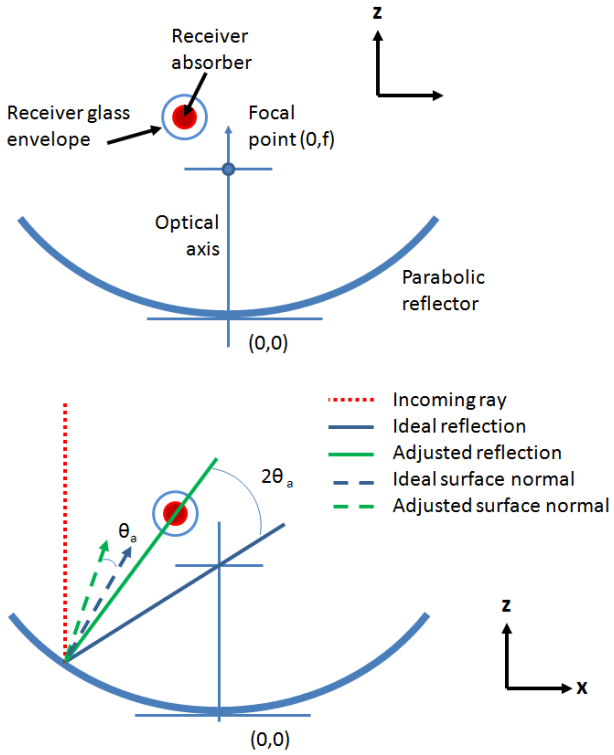

FIGURE 2. DEPICTION OF ABSORBER MISALIGNMENT REPRESENTED WITH EFFECTIVE SLOPE ERRORS

The effective slope errors for a misaligned absorber depend on both the magnitude and direction of displacement. Figure 3 illustrates eight directional absorber misalignments. Varying the displaced distance and the direction provides an understanding of the magnitude of effective slope errors due to absorber misalignments. For an LS-2 geometry collector (5 m aperture, 1.49 m focal length, and 7 cm diameter absorber), Fig. 4 shows the effective slope errors for absorber misalignments between 1 and 3 cm in each of the eight sampled directions. Through examination of Fig. 4, it is apparent that absorber displacements as small as 1 cm result in equivalent slope errors of over 3 mrad, while larger displacements of 3 cm are equivalent to slope errors as large as 10 mrad. Small imperfections from manufacturing and assembly can easily introduce localized slope errors equal or greater than 3 mrad in the most accurate of parabolic collectors. Thus small absorber displacements become at least as significant as reflector slope errors. The implication strengthens the case for the proposed technique.

1.3 Absorber Alignment Measurement Method

The absorber alignment is measured by taking two photographs of the entire collector, including the absorber, from each

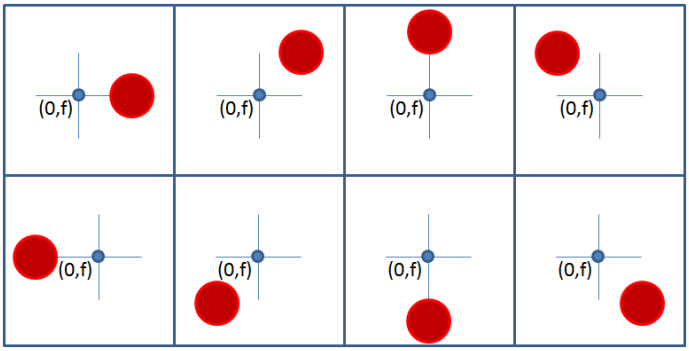

FIGURE 3. SAMPLE OF EIGHT POSSIBLE DIRECTIONAL ABSORBER MISALIGNMENTS

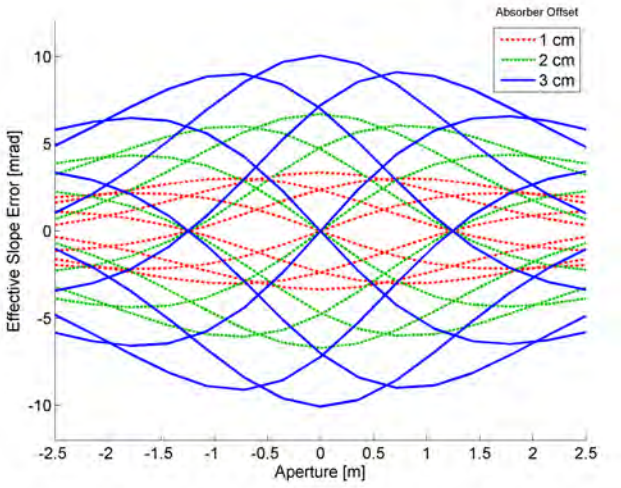

FIGURE 4. EFFECTIVE SLOPE ERRORS FOR MISALIGNMENTS WITH 1-3 cm DISPLACEMENTS FROM THE FOCAL POINT. MULTIPLE LINES OF THE SAME COLOR REPRESENT DIRECTIONAL DISPLACEMENTS IN THE EIGHT DIRECTIONS SHOWN IN FIG. 3

side of the aperture. Through use of photogrammetry, explained in detail later, a photograph of the absorber taken from a known camera position can be used to measure the projection of the absorber onto a chosen plane. While any plane is acceptable, a plane parallel to the aperture and through the focal line of the collector (focal-line plane) is a logical choice given that we are interested in the position of the absorber relative to the focal line. The location of the camera (X_c, Z_c), the location of the projection of the absorber onto the focal-line plane (X_f, Z_f), and the location of the absorber (X_a, Z_a) are related by similar triangles given in Eqn. 3 and shown in Fig. 5.

$$\frac{Z_c - Z_f}{X_c - X_f} = \frac{Z_f - Z_a}{X_f - X_a} \tag{3}$$

As the location of the camera and the location of the projection of the absorber can both be determined from the photograph, the two remaining unknowns are the location of the absorber in two dimensions (X_a, Z_a). Two photographs taken from different angles (as shown in Fig. 5) provide a system of two equations with two unknowns that can be solved explicitly for the absorber location. Taking more than two photographs allows for a least squares solution, thus improving the accuracy of the measurement. The essence of this method thus reduces to determination of the location of the camera and the location of the projection of the absorber from a photograph. A digital camera, four photogrammetry targets, a distance measurement device, and a calibration target are required for this process. The camera is calibrated before use to characterize the focal length, principal point, and lens distortion parameters. The four targets are placed at the corners of the collector, and the distances between them are measured using a laser distance meter. Two photographs are then taken of the collector and absorber, one from each side of the aperture. The camera position for each photograph is determined from the measured location of the targets, the location of the targets in the photograph, and the camera calibration parameters. The photographs are re-sampled on a regular grid of points across the focal-line plane of the collector. The centerline of the absorber is then determined by image processing each re-sampled photograph. The absorber position is ultimately determined from both photographs, given known camera locations and the locations of the projection of the absorber onto the focal-line plane of the collector.

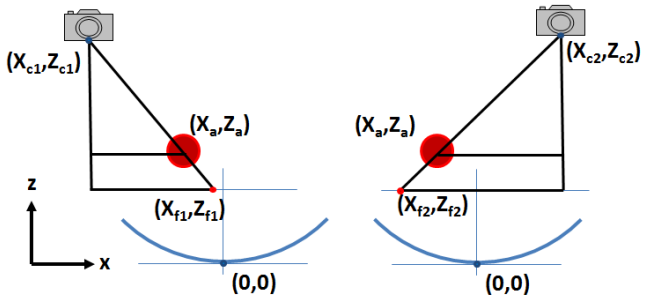

FIGURE 5. RELATIONSHIP BETWEEN THE ABSORBER LOCATION (X_a, Z_a), THE PROJECTION OF THE ABSORBER ONTO THE FOCAL-LINE PLANE (X_f, Z_f), AND THE CAMERA POSITION (X_c, Z_c)

1.4 Camera Model

In order to use a camera as a tool to measure the absorber alignment, the camera must be well characterized. Traditionally, cameras are modeled using a perspective-center model to

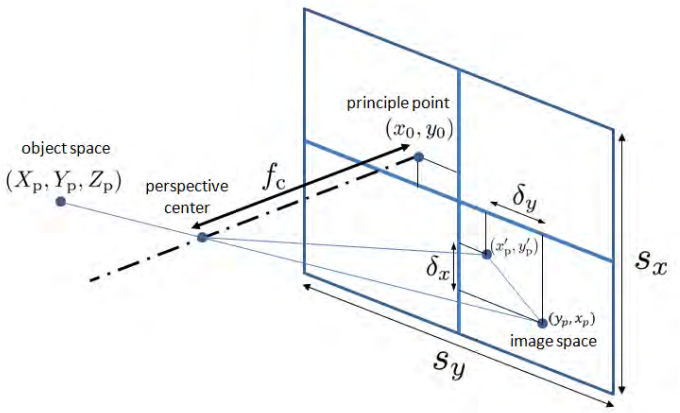

FIGURE 6. PERSPECTIVE-CENTER MODEL OF A CAMERA

which both radial and tangential lens distortions are applied. The perspective-center model is based on the principle of collinearity; that is, a point in object space, the corresponding point on the image sensor (image space), and the focal point of the camera all lay on a straight line. Object space is the 3D space containing the objects that you are photographing, while image space is the 2D image sensor in the camera. The principle of collinearity allows the location of points in object space to be determined from their corresponding locations in image space, which is how the absorber alignment is measured. Figure 6 illustrates the perspective-center camera model. The object point (X_p, Y_p, Z_p) is imaged by the real camera on the sensor at point (x'_p, y'_p). This image point must be corrected by the lens distortion components (δ_x, δ_y) so that it is imaged by the perspective-center camera at point (x_p, y_p). The sensor size (s_x x s_y) is the length and height of the image sensor. The perspective center is the point through which all straight lines pass. The principal point (x_0, y_0) is the intersection of the image sensor and a line perpendicular to the image sensor passing through the perspective center. The focal length (f) is the normal distance between the image sensor and the perspective center. The lens distortion quantifies the deviation of rays from the ideal central-perspective model in a real camera and is expressed as deviations (δ_x, δ_y) in the image plane. The primary types of lens distortion are radial distortion and tangential distortion. Radial distortion accounts for the majority of lens aberrations and has radial symmetry, while tangential distortion is mainly caused by decentering or misalignment of lens elements. There are three radial distortion coefficients (K_1, K_2, and K_3) that are used to determine the radial components of distortion

$$\begin{aligned} \delta_{x_r} &= x'(K_1 r^2 + K_2 r^4 + K_3 r^6) \\ \delta_{y_r} &= y'(K_1 r^2 + K_2 r^4 + K_3 r^6) \end{aligned} \tag{4}$$

where any point (x', y') on the image sensor can be described as

$$r = \sqrt{x'^2 + y'^2} \tag{5}$$

The tangential distortion coefficients (P_1 and P_2) are used to determine the tangential components of distortion.

$$\begin{aligned} \delta_{x_t} &= P_1(r^2 + 2x'^2) + 2P_2 x' y' \\ \delta_{y_t} &= P_2(r^2 + 2y'^2) + 2P_1 x' y' \end{aligned} \tag{6}$$

The radial and tangential components of lens distortion are summed to determine the total distortion displacement in each direction.

$$\begin{aligned} \delta_x &= \delta_{x_r} + \delta_{x_t} \\ \delta_y &= \delta_{y_r} + \delta_{y_t} \end{aligned} \tag{7}$$

To correct for lens distortion the pixel positions are shifted by the total distortion displacement values. This transforms the image to emulate one obtained by a central perspective camera.

$$\begin{aligned} x &= x' + \delta_x \\ y &= y' + \delta_y \end{aligned} \tag{8}$$

Therefore, a point in object space (X, Y, Z) will appear on the real camera's sensor in image space at (x', y'). Once the camera is modeled as a perspective-center camera, where the point in object space, the focal point, and the point in image space are collinear, the point in image space is corrected to be located at (x, y). A photograph that appears as though it were taken with a perspective-center camera is called an ideal photograph. Real photographs can be corrected to ideal photographs after a camera calibration is used to quantify the camera geometry.

2 Data Collection

2.1 Camera Calibration

The first step in using the absorber alignment method is to calibrate the camera that will be used to photograph the absorber. A complete camera calibration quantifies the focal length, sensor size, principal point of the camera, and both the radial and tangential lens distortion coefficients. Specifications provided by the camera manufacturer for sensor size and focal length are approximations and should not be used in calculations; these values should always be determined with a camera calibration.

The camera is calibrated by taking images of a calibration target. A grid of dots or a black and white checkerboard, as shown in Fig. 7, are convenient targets for calibration. A camera

calibration toolbox for Matlab developed by CalTech is available online [8], or a commercial software package, such as PhotoModeler [9], can be purchased to perform the calibration. The advantage of the PhotoModeler software is that the geometry of the calibration target need not be known but can be calculated during the calibration process using bundle adjustment. Other commercial photogrammetry software packages exist that are capable of performing camera calibrations, but the authors' experience is limited to the previously mentioned options. Specific guidelines for each of the aforementioned camera calibration platforms are provided with each software package.

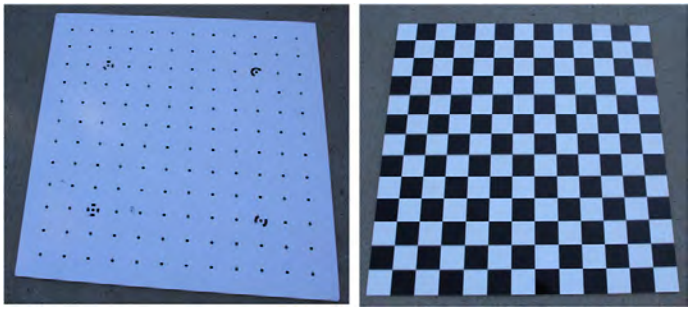

FIGURE 7. PHOTOGRAPHS OF EXAMPLE CALIBRATION TARGETS

2.2 Target Layout

Four black circular targets mounted on a white background are affixed to the four corners of the collector. It is important to use targets made of felt or special light-absorbing flocked black paper so that the targets do not appear faded due to large amounts of reflected light common with printed targets. The targets' diameter sized in image-space should span about 10 pixels. If the target size is too great, centroiding error is introduced by the elliptical shape of the targets in the images. If too small, then accuracy suffers due to poorly resolved target images. Once the targets are in place, the six distances between these four targets (Fig. 8) should be physically measured with a laser distance meter. The photogrammetry targets' locations are represented as (X_{pi}, Y_{pi}) where $i = 1,2,3,4$ for each of the four targets. The targets are assumed to lie within the same Z-plane parallel to the aperture of the collector. For a collector with aperture width w_{ap}, length l_c, and target radius r_t, the coordinate system is determined by defining the location of the first target in both x- and y-coordinates $\left((X_{p1}, Y_{p1}) = (-w_{ap}/2 + r_t, -l_c/2 + r_t)\right)$ and the second target in the y-coordinate ($Y_{p2} = l_c/2 - r_t$). This frame thus defines the system's translation and rotation. There are five remaining unknowns $(X_{p2}, X_{p3}, Y_{p3}, X_{p4}, Y_{p4})$ and six equations (Eqn. 9) provided by the distance measurements.

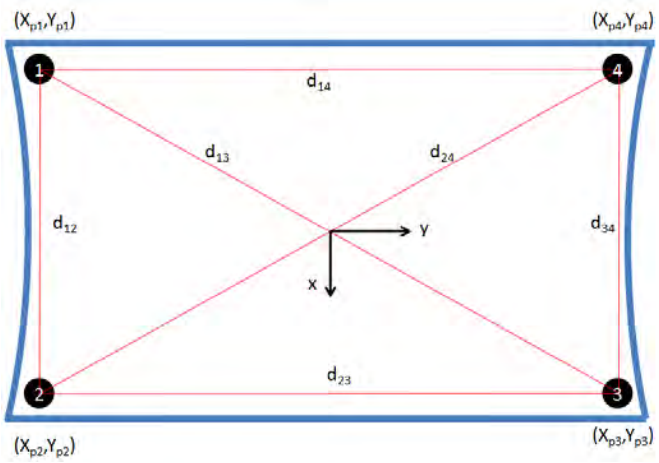

FIGURE 8. TARGET PLACEMENT FOR THE FOUR TARGETS (X_{pi}, Y_{pi}) AND LOCATIONS OF THE SIX DISTANCE MEASUREMENTS $(d_{i,j})$

$$(X_{pi} - X_{pj})^2 + (Y_{pi} - Y_{pj})^2 - d_{ij}^2 = 0 \quad \text{for } i \neq j \text{ where } i = 1..4,\ j = 1..4 \tag{9}$$

The system of equations can therefore be solved by only taking five of the distance measurements; however, using all six allows for a least squares solution, thus improving the target location accuracy.

2.3 Photo Acquisition

Once the targets have been affixed to the corners of the collector, the measurement photographs can be taken. The photographs should be taken such that the four targets fill as much of the image as possible. A minimum of two photographs, one from each side of the aperture, should be taken as shown in Fig. 5. The best locations from which to take the photographs are at 45° angles from the vertex of the collector because the uncertainty in the absorber location measurement is minimized at that location. For example, if the camera is positioned 10 m above the vertex of the collector (Z_c = 10 m), it should be located 10 m away from the collector's vertex (X_c = 10 m) or 7.5 m past the rim on either side for a 5 m aperture collector.

3 Image Processing

3.1 Idealization of Photographs

Before a photograph can be analyzed, it must be corrected for lens distortion. The most accurate method to remove lens distortion is to resample the photograph, thereby creating an

ideal photograph that appears as though it were taken with a perspective-center camera with no lens distortion. All processing is then performed on the ideal photograph. Lens distortion can also be removed after image processing of the original photograph. This method offers improvements in speed in exchange for a slight decrease in accuracy. However, since only two photographs are used in this absorber alignment measurement technique, the reduction in speed is inconsequential. Thus the most accurate method, correcting the lens distortion before processing the image, is used. To create an ideal photograph, the location of each pixel on the sensor is shifted to correct for the lens distortion and principal point offset (x_0, y_0). The locations in image space (x'_{p}, y'_{p}) of the pixels in a real photograph are distributed uniformly across the image sensor. For a photograph with $N_{\mathrm{p_x}}$ pixels in the vertical direction and $N_{\mathrm{p_y}}$ pixels in the horizontal direction and a sensor size of s_{x} by s_{y}, the index of each pixel in the photograph is given as ($x_{\mathrm{I}}, y_{\mathrm{I}}$) and the locations in image space are calculated as

$$\begin{aligned} x'_{\mathrm{p}} &= x_{\mathrm{I}} \quad \frac{s_{\mathrm{x}}}{N_{\mathrm{p_x}}} \quad - x_0 \\ y'_{\mathrm{p}} &= y_{\mathrm{I}} \quad \frac{s_{\mathrm{y}}}{N_{\mathrm{p_y}}} \quad - y_0 \end{aligned} \tag{10}$$

The pixel locations in image space for the ideal photograph (x_{p},y_{p}) are determined by shifting the pixel locations for the real photograph by the total lens distortion displacement in each direction as given in Eqn. 11.

$$\begin{aligned} x_p &= x'_{\mathrm{p}} + \delta_{\mathrm{x}} \\ y_p &= y'_{\mathrm{p}} + \delta_{\mathrm{y}} \end{aligned} \tag{11}$$

An ideal photograph is then created by determining the intensity value on the photograph at the ideal pixel locations. The intensity values are determined by interpolation. The authors use Delaunay triangulation to perform the interpolation. Alternative interpolation routines can be used with different trade-offs in speed and accuracy.

3.2 Target Centroiding

Using an ideal photograph as described above, the centroid of the four circular targets must be determined. Any centroiding algorithm may be used; however, the uncertainty in the absorber location depends on the accuracy of the method employed. For this purpose, the authors developed a code that extracts contour lines (level sets) in the target region using a marching squares algorithm. An ellipse is fit to each contour line, and the centers of the ellipses are averaged to determine the centroid. Figure 9 shows an image of a target that is about 20 pixels in diameter (slightly larger than ideal). The contour lines are overlaid on the image in blue, and the ellipses fit to those contour lines appear in red. The averaged center of the ellipses is shown as a white dot.

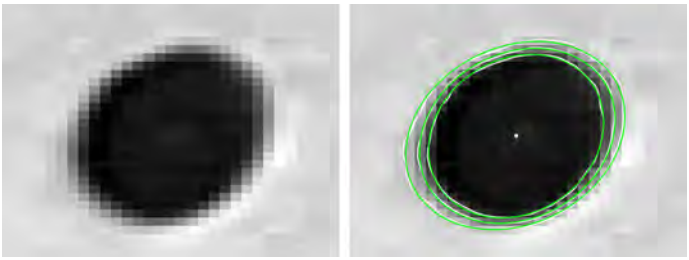

FIGURE 9. IMAGE OF TARGET (TOP) WITH OVERLAID CONTOUR LINES IN BLUE AND ELLIPSES IN RED (BOTTOM)

3.3 Camera Location

Using the four measured target locations and the four target centroid locations for each photograph, the camera positions are calculated by photogrammetric resection. The well-known collinearity equations describe the relationship between target locations in object space and the corresponding target locations in image space [10]. The camera location in object space is defined by six independent parameters called the external orientation parameters: the camera position in three dimensions ($X_{\mathrm{c}}, Y_{\mathrm{c}}, Z_{\mathrm{c}}$) and the direction the camera is pointing described by a rotation matrix (R) with elements $r_{i,j}$, representing rotation by Euler angles ($\theta_\alpha, \theta_\beta, \theta_\gamma$). The target locations are described in three-dimensional object space ($X_{\mathrm{p}}, Y_{\mathrm{p}}, Z_{\mathrm{p}}$) and in two-dimensional image space ($x_{\mathrm{p}}, y_{\mathrm{p}}$). The camera geometry is defined by the internal orientation parameters, where (x_0, y_0) and f_{c} are the locations of the principal point on the image sensor and the focal length of the camera, respectively. The images should already have been corrected for lens distortion as described above.

$$\begin{aligned} x_{\mathrm{p}} - x_0 &= -f_{\mathrm{c}} \frac{r_{11}(X_{\mathrm{p}} - X_{\mathrm{c}}) + r_{12}(Y_{\mathrm{p}} - Y_{\mathrm{c}}) + r_{13}(Z_{\mathrm{p}} - Z_{\mathrm{c}})}{r_{31}(X_{\mathrm{p}} - X_{\mathrm{c}}) + r_{32}(Y_{\mathrm{p}} - Y_{\mathrm{c}}) + r_{33}(Z_{\mathrm{p}} - Z_{\mathrm{c}})} \\ y_{\mathrm{p}} - y_0 &= -f_{\mathrm{c}} \frac{r_{21}(X_{\mathrm{p}} - X_{\mathrm{c}}) + r_{22}(Y_{\mathrm{p}} - Y_{\mathrm{c}}) + r_{23}(Z_{\mathrm{p}} - Z_{\mathrm{c}})}{r_{31}(X_{\mathrm{p}} - X_{\mathrm{c}}) + r_{32}(Y_{\mathrm{p}} - Y_{\mathrm{c}}) + r_{33}(Z_{\mathrm{p}} - Z_{\mathrm{c}})} \end{aligned} \tag{12}$$

where

$$\mathbf{R} = \begin{bmatrix} r_{11} & r_{12} & r_{13} \\ r_{21} & r_{22} & r_{23} \\ r_{31} & r_{32} & r_{33} \end{bmatrix} =$$

$$\begin{bmatrix} \cos\theta_\gamma & -\sin\theta_\gamma & 0 \\ \sin\theta_\gamma & \cos\theta_\gamma & 0 \\ 0 & 0 & 1 \end{bmatrix} \begin{bmatrix} 1 & 0 & 0 \\ 0 & \cos\theta_\alpha & -\sin\theta_\alpha \\ 0 & \sin\theta_\alpha & \cos\theta_\alpha \end{bmatrix} \begin{bmatrix} \cos\theta_\beta & 0 & -\sin\theta_\beta \\ 0 & 1 & 0 \\ \sin\theta_\beta & 0 & \cos\theta_\beta \end{bmatrix}$$

To solve for the external orientation parameters, the collinearity equations are linearized using a first-order Taylor series expansion. Since each target provides two equations, three targets are required to explicitly solve for the six unknowns. Using more than three targets (four in this case) allows for a least squares solution to provide a best estimate of the external orientation parameters.

3.4 Projection of the focal-line plane

Once the camera location is known, the projection of the absorber onto the focal-line plane can be measured in each photograph. A regular grid of points is created at the focal line of the collector, perpendicular to the optical axis (focal-line plane) as shown in Fig. 10. The parabolic trough reflector is also discretized; although the reflector points are not used to find the receiver location, they are useful here as a visual guide. The

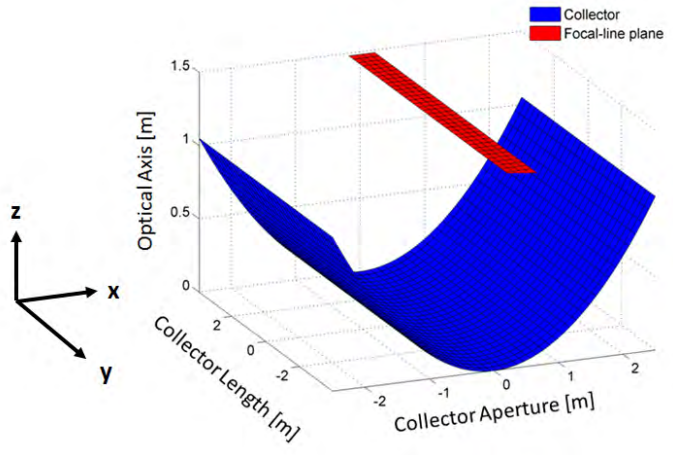

FIGURE 10. REGULAR GRID OF POINTS DISCRETIZING THE PARABOLIC COLLECTOR AND THE FOCAL-LINE PLANE

points along the focal line are object points because their locations are determined in 3D object space. To project an object point (X_p, Y_p, Z_p) onto a photograph, both the external orientation parameters and the internal orientation parameters of the camera must be known. The collinearity equations (Eqn. 12) can then be solved explicitly for the corresponding image points on the sensor (x_p, y_p). Points in image space can be converted to pixel space (x_I, y_I) by shifting them by half the sensor length and then scaling by the ratio of the number of pixels (N) to the length of the sensor (s) (Eqn. 14).

$$x_\mathrm{I} = \left(x_\mathrm{p} + \frac{s_\mathrm{x}}{2}\right) \quad \frac{N_\mathrm{px}}{s_\mathrm{x}} \tag{13}$$

$$y_\mathrm{I} = \left(y_\mathrm{p} + \frac{s_\mathrm{y}}{2}\right) \quad \frac{N_\mathrm{py}}{s_\mathrm{y}} \tag{14}$$

Figure 11 shows a photograph of a collector with the receiver

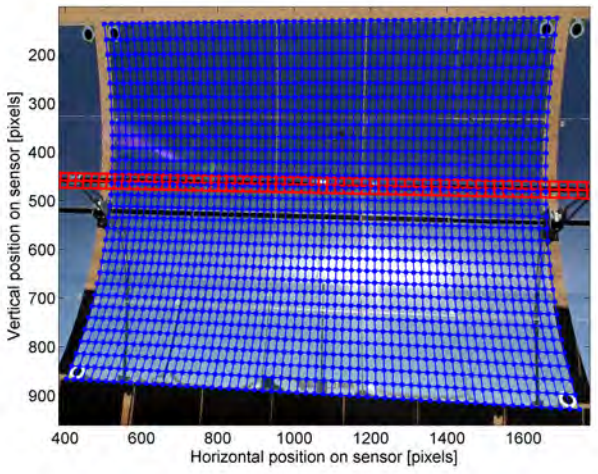

FIGURE 11. IDEAL PHOTOGRAPH WITH REGULAR GRID OF POINTS PROJECTED ONTO THE COLLECTOR AND THE FOCAL-LINE PLANE

and reflector discretizations superimposed on it. The intensity values at the location of each point on the focal-line grid are determined by interpolating the intensity values in the photograph. The technique is the same that was used to create an ideal photograph by re-sampling the original photograph at the corrected pixel locations. Re-sampling the photograph along the focal-line grid corrects for the effects of parallax and results in an image of the focal-line plane where the location of each image pixel is known relative to the collector. Figure 12 shows the resulting image of the absorber at the focal-line plane. Since this image is centered on the focal line, the location of the absorber in the image indicates the measured offset of the absorber projected onto the focal-line plane.

3.5 Locating the centerline of the absorber image

Image processing is used to find the centerline of the absorber in Fig. 12. Once the location of the centerline is known in pixels it can be directly converted to an offset from the focal

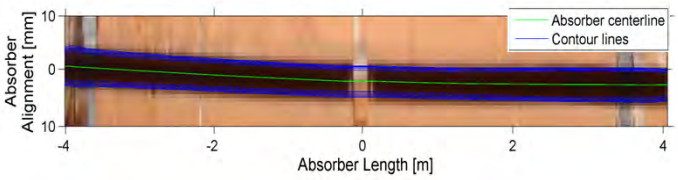

FIGURE 12. PARALLAX CORRECTED PHOTOGRPAH OF THE FOCAL-LINE PLANE SHOWING THE ABSORBER

line in millimeters given that the image of the absorber was created on a known uniform grid. Similar to the first step in finding the target centroids, contour lines (level set) are used to find the centerline of the absorber. The photograph is first filtered to remove the gap in the image of the absorber due to the receiver support. Lines of constant intensity are then calculated for each color plane of the image. The lines are filtered to remove noise and false edges. The remaining contour lines are averaged to find the centerline of the absorber. Figure 12 shows the image of the absorber overlaid with the final contour lines and the averaged centerline.

4 Experiment

4.1 Experimental Setup

To demonstrate the accuracy of this method, an outdoor test stand was developed to mimic the geometry of a parabolic collector and absorber. Four targets are placed at the corners of a 5 m x 8 m rectangle on the ground mimicking the aperture plane of an LS-2 type collector. Three sections of 3 m long steel pipe with an outer diameter of 73 mm are used to represent the 70 mm-diameter absorbers. The setup is shown in Fig. 13. The distances between the targets are measured using a Leica Disto D5 laser distance meter with accuracy ± 1.5 mm. A camera mounted on an extendable mast is used to take photographs of the setup from both sides of the aperture. The photographs are taken at a height of 10 m and a horizontal distance of 10 m from the absorber. The camera is a Nikon D300 with a 20 mm fixed focal length lens. The photographs are processed to determine the camera location for each photograph and then the absorber location in two dimensions.

4.2 Measurement Validation

To determine the accuracy of this method, the absorber location is also measured using traditional photogrammetry. About 30 additional targets are placed within the 5 m x 8 m rectangle along with 15 targets on the top of the absorber in line horizontally with the center of the tube. A set of between 20 and 40 photographs are taken of the setup from all sides at a height of about 10 m. A commercial photogrammetry packet, PhotoModeler, is used to process the photographs and determine the 3D

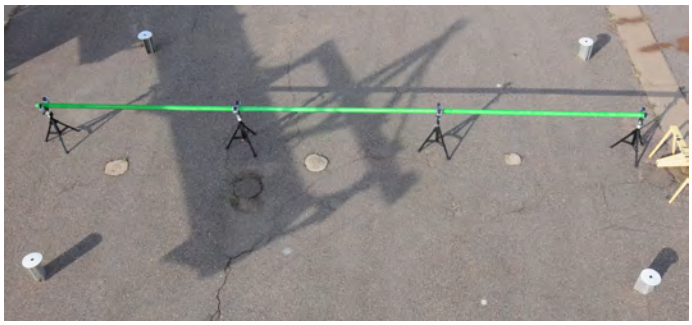

FIGURE 13. ABSORBER ALIGNMENT MEASUREMENT TEST SETUP WITH FOUR TARGETS AND MOCK ABSORBER

location of each point. The points on the absorber tube are adjusted by the absorber radius to account for the fact that they are located on top of the absorber and not at its center line. Linear interpolation is used to determine the location of the absorber between the photogrammetry points. The photogrammetry results are then compared to the absorber alignment measurement results.

Three different horizontal (X_a) absorber locations and three different vertical (Z_a) absorber locations were measured using both the absorber alignment measurement technique and photogrammetry. Figures 14 and 15 show the absorber positions in the horizontal and vertical dimensions, respectively, for those tests in which the absorber is moved in that dimension. The dashed line represents interpolation between the photogrammetry points shown as dots, while the solid lines represent the absorber alignment measurement results. For all five test cases along the full length of the absorber, the absorber alignment method compares with the linear fit to photogrammetry points with a pooled standard deviation of ± 2.1 mm in the horizontal dimension and ± 0.9 mm in the vertical dimension.

4.3 Uncertainty

By comparing the absorber alignment measurement to a well characterized measurement method, photogrammetry, the uncertainty analysis is greatly simplified. The sources of uncertainty to be quantified are the uncertainty in the placement of the photogrammetry targets relative to the absorber centerline, the uncertainty in the location of those points calculated with photogrammetry, and the difference between the photogrammetry absorber location and the absorber alignment measurement. The uncertainty values for each source are listed in Tab. 2. The total uncertainty in the absorber alignment measurement is thus ± 4.7 mm and ± 2.2 mm in the x- and z-dimensions, respectively.

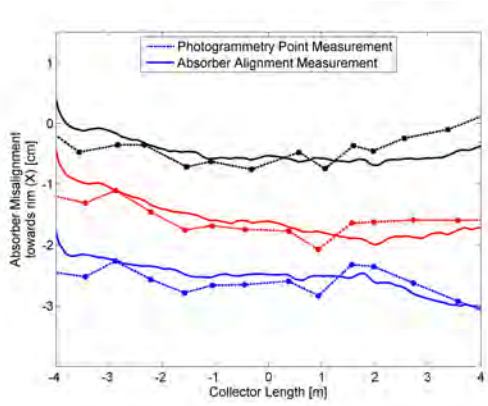

FIGURE 14. ABSORBER ALIGNMENT IN THE HORIZONTAL DIMENSION FROM PHOTOGRAMMETRY (DOTS), INTERPOLATION BETWEEN PHOTOGRAMMETRY POINTS (DASHED LINED), AND ABSORBER ALIGNMENT MEASUREMENT (SOLID LINE)

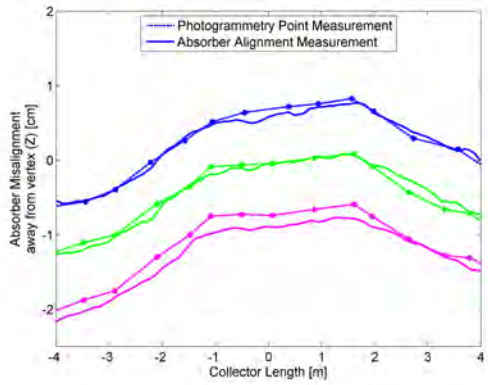

FIGURE 15. ABSORBER ALIGNMENT IN THE VERTICAL DIMENSION FROM PHOTOGRAMMETRY (DOTS), INTERPOLATION BETWEEN PHOTOGRAMMETRY POINTS (DASHED LINED), AND ABSORBER ALIGNMENT MEASUREMENT (SOLID LINE)

5 Field Results

One simple application of the absorber alignment measurement technique is to measure the absorber alignment as a function of the gravitational loading. While there is some prior work using Finite Element Analysis to determine the effects of gravitational loading on reflector slope errors [11], there is no mention of the effects of gravity on absorber alignment.

As the parabolic trough tracks the sun from east to west throughout the day, the orientation of the collector frame and absorber with respect to gravity both change. Figure 16 shows three different collector orientations along with exaggerated expected absorber misalignments due to gravity (g). The absorber alignment measurement technique was used to measure the absorber alignment of a prototype parabolic collector at its extreme positions: 0° (facing East), 90° (facing straight up), and 170° (facing West). The tracker capabilities prevented testing a true west orientation of 180°. The absorber position perpendicular to the optical axis (X-dimension) changed by a maximum of about 6 cm between 0° and 170° shown in Fig. 17. The absorber position along the optical axis (Z-dimension) did not change significantly between different collector orientations. The direction of these absorber misalignments conform to expectations; for orientations of 0° and 170° the absorber shifts in the direction of gravity. Likewise, minimal changes in the absorber position along the optical axis result from the fixed length of the receiver supports. These results show both the importance and value of measuring the absorber alignment. Since the collector tested was a prototype, the stiffness of the frame and receiver supports can be improved in future generations of the collector to prevent absorber misalignments.

TABLE 2. UNCERTAINTY COMPONENTS OF ABSORBER ALIGNMENT MEASUREMENT

	Towards collector rim (X)		Away from collector vertex (Z)	
	Random (95%)	Systematic (95%)	Random (95%)	Systematic (95%)
Placement of photogrammetry targets relative to centerline of absorber	+/- 2mm	-	+/- 1mm	-
Location of photogrammetry targets measured with photogrammetry	+/- 0.7 mm	-	+/- 0.8 mm	-
Difference between photogrammetry results and absorber alignment measurement results	+/- 4.2 mm	+/- 0.2 mm	+/- 1.8 mm	+/- 0.4 mm
Totals	4.7	0.2	2.2	0.4
	4.7		2.2	

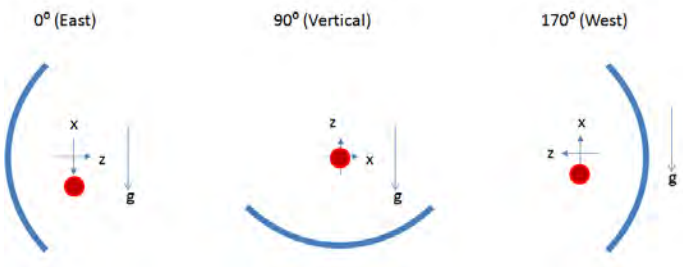

FIGURE 16. GRAVITATIONAL LOADING AND EXPECTED ABSORBER MISALIGNMENT FOR DIFFERENT COLLECTOR ORIENTATIONS

6 Conclusions

A simple technique has been developed to measure the absorber alignment in parabolic trough solar collectors. This

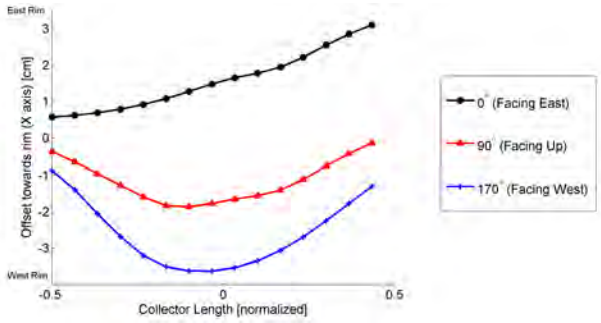

FIGURE 17. ABSORBER ALIGNMENT PERPENDICULAR TO THE OPTICAL AXIS (X-DIMENSION) FOR THREE DIFFERENT COLLECTOR ORIENTATIONS

method uses a calibrated digital camera to take two photographs of the collector and absorber assembly, one from each side of the aperture. Four photogrammetry targets mounted on the corners of the collector are used to determine the camera location with photogrammetric resection. The absorber alignment is then determined by calculating the location of the projection of the absorber onto the focal-line plane in each photograph and solving a linear system of equations. An outdoor full-scale test was performed with a mock absorber to determine the accuracy of the absorber alignment measurement method. This measurement was compared with a photogrammetric measurement of a series of targets placed directly on the absorber. The overall uncertainty in the absorber alignment measurement was determined to be ± 4.7 mm and ± 2.2 mm in the x- (towards the rim) and z-dimensions (along the optical axis), respectively. The absorber alignment measurement technique was then used in the field to measure the absorber alignment at different collector orientation angles to determine the effect of gravitational loading on the absorber alignment. The results of this test show an absorber displacement in the direction perpendicular to the optical axis (towards the rim) of up to 5 cm between an east-facing and a west-facing collector. The ability to simply and easily measure the absorber position of a parabolic trough solar collector in the field will thus be valuable for both research and development of future parabolic collectors and evaluation of current collector designs.

ACKNOWLEDGMENT

This work was supported by the U.S. Department of Energy under Contract No. DE-AC36-08-GO28308 with the National Renewable Energy Laboratory.

REFERENCES

[1] Treadwell, G. W., 1976. Design considerations for Parabolic-Cylindrical solar collectors. Tech. Rep. SANd76-0082, Sandia National Laboratories, Albuquerque, NM, July.

[2] Treadwell, G. W., and Grandjean, N. R., 1981. Systematic rotation and receiver location error effects on parabolic trough annual performance. Tech. Rep. SAND81-0159, Sandia National Laboratories, Albuquerque, NM, Apr.

[3] Ulmer, S., Heinz, B., Pottler, K., and Lüpfert, E., 2009. "Slope error measurements of parabolic troughs using the reflected image of the absorber tube". *Journal of Solar Energy Engineering,* ***131***.

[4] Schiricke, B., Pitz-Paal, R., Lüpfert, E., Pottler, K., Pfänder, M., Riffelmann, K. J., and Neumann, A., 2009. "Experimental verification of optical modeling of parabolic trough collectors by flux measurement". *Journal of Solar Energy Engineering,* ***131***.

[5] Wendelin, T., May, K., and Gee, R., 2006. "Video scanning hartmann optical testing of State-of-the-Art parabolic trough concentrators". In Proceedings of the ASME 2006 International Solar Energy Conferencer.

[6] Andraka, C. E., Sadlon, S., Myer, B., Trapeznikov, K., and Liebner, C., 2009. "Rapid reflective facet characterization using fringe reflection techniques". In Proceedings of the ASME 2009.

[7] Pottler, K., Lüpfert, E., Johnston, G. H., and Shortis, M. R., 2005. "Photogrammetry: A powerful tool for geometric analysis of solar concentrators and their components". *Journal of Solar Energy Engineering,* ***127***, p. 94.

[8] Bouguet, J., 2010. Camera calibration toolbox for matlab. http://www.vision.caltech.edu/bouguetj/calib_doc/, July.

[9] Inc., E. S., 2011. PhotoModeler. http://www.photomodeler.com/index.htm.

[10] Wong, K. W., 1980. "Basic mathematics of photogrammetry". In *Manual of Photogrammetry*, C. Slama, C. Theurer, and S. Henriksen, eds., 4th ed. American Society of Photogrammetry and Remote Sensing.

[11] Christian, Joshua, M., and Ho, Clifford, K., 2011. "Finite element modeling and ray tracing of parabolic trough collector for evaluation of optical intercept factor with gravity loading". In Proceedings of the ASME 5th International Conference on Energy Sustainabiliby.